

Three areas in the south are thickening at rates of up to 25 cm/year (centered near 68°N 319°E, 67°N 314°E, and 63°N 313°E in Fig. 1). The two northernmost of these show reasonable agreement with results from satellite radar-altimeter data (1), with thickening rates in the east increasing to more than 15 cm/year nearer the coast. In the south, thickening rates reach maximum values of 25 cm/year. All three thickening zones are in regions of high snowfall (4), with accumulation rates strongly linked to storm intensity and subject to considerable interannual variability. However, model studies (4) conclude that precipitation over this region should have decreased significantly between 1985 and 1995, which would have resulted in thinning. In the northwest, where repeat radar-altimeter data (1) and comparison of snow accumulation with ice discharge (5) have shown previous thinning, we observe a slight thickening. This could represent a change in conditions with time.

In the peripheral regions, we observe large areas of thinning, with thinning rates increasing rapidly toward the ocean (Fig. 1). We observe thinning of up to 20 cm/year over an area centered near 69°N 313°E and at far higher rates near the coast in the southwest and in the east. There is a remarkably sharp transition from thickening in the west to thinning in the east almost exactly along much of the ice-sheet ridge where it runs north-south.

Our results agree broadly with those from radar-altimeter data (1) for the east of the summit ridge but include data from a far larger area. Most rapid thinning rates (more than 1 m/year) were observed in the lower reaches of east coast outlet glaciers. Our results give an average thickening (without correcting for vertical crustal motion), for elevations above 2000 m, of 0.5 ± 0.7 cm/year for 1993 to 1998, which is smaller than the most recently published average thickening value of 2.2 ± 0.9 cm/year between 1978 and 1988 estimated from satellite radar-altimeter data for the same region (1). However, neither of the error estimates includes errors associated with interpolating between flight lines, and that for the radar-altimeter data includes only the random component of the error (1). Consequently, these higher elevation central regions could have been almost exactly in balance for the past 20 years, or they could be shifting from slight thickening to a balanced condition.

The lower elevation coastal regions are behaving differently. Thickening and thinning rates for all surfaces below 2000 m show extensive thinning in the east (Fig. 2), consistent with observations of warmer than normal temperatures for 1993 to 1998. However, we also observed areas of thinning near the west coast (Fig. 1), where many locations were cooler than normal (6). The elevation changes along the west and south sides of the ice sheet (Fig. 1) show good qualitative agreement with esti-

mates of marginal ice advance and retreat between 1950 and 1985 based on comparison of aerial photographs (7), but not along the east coast, where the earlier, rather sparse data suggest glacier advance between 1950 and 1985.

We observed the highest rates of thinning in the lower reaches of outlet glaciers along the east coast, where we might expect large changes caused by interannual variability in melt rates (8). Over the 5-year period, total thinning of as much as 10 m was observed in the lower reaches of all east coast outlet glaciers that were surveyed, at latitudes up to 69°N and at surface elevations up to 1500 m (Fig. 2). The observed thinning could be explained by a reduction in snowfall or by an increase in summer melting of as much as a 10-m ice equivalent over the 5-year period. This represents a sustained perturbation of 100% or more and is extremely unlikely. Consequently, we believe the glaciers to be thinning as a result of increased creep rather than because of excessive melting or decreased snowfall. This raises the possibility that the basal friction of these glaciers has decreased, possibly because of an increase in the amount of surface melt water penetrating to the bed of the glacier. If this is correct, it would represent a mechanism for transfer of ice-sheet mass to the oceans that is potentially larger than could be achieved by surface melting alone.

These observations of extensive, near-coastal thinning of the Greenland ice sheet illustrate the importance of detailed monitoring of these regions. The airborne surveys reported here, and those to be repeated in

1999, will establish baseline data sets, which will be extended with information from NASA's ICESAT (9). This satellite laser altimeter will be launched in 2001 to measure ice-surface elevations in Greenland and Antarctica at all latitudes up to 86°.

References and Notes

1. C. H. Davis, C. A. Kluever, B. Haines, *Science* **279**, 2086 (1998); H. J. Zwally, A. C. Brenner, J. P. DiMarzio, *ibid.* **281**, 1251 (1998).
2. W. B. Krabill, R. H. Thomas, C. F. Martin, R. N. Swift, E. B. Frederick, *Int. J. Remote Sens.* **16**, 1211 (1995).
3. C. W. Wright, *Proc. SPIE Conference*, Orlando, FL (Bellingham, Washington, DC, 1992), pp. 2-7.
4. D. H. Bromwich *et al.*, *J. Geophys. Res. Atmos.* **103**, 26007 (1998).
5. R. H. Thomas *et al.*, *J. Glaciol.*, in press.
6. W. Abdalati, personal communication (October 1998). Summer temperatures (June, July, and August) were averaged for 1993 to 1997 and compared with average summer temperatures for 1979 to 1997 to show an increase on the east coast of about 0.3°C and a similar decrease along much of the west coast. Data from 19 coastal stations were used.
7. A. Weidick, *Rapp. Gronlands. Geol. Unders.* **152**, 73 (1991).
8. R. J. Braithwaite, *Global Planet. Change* **9**, 251 (1994).
9. Schutz, B., *Proc. Wegener-98*, Krokkeiva, Norway (Norwegian Mapping Authority, Hønefoss, Norway, 1998).
10. Supported by NASA's Polar Research Program and ICESAT Project. We thank the crew of the NASA P-3 aircraft used for the Greenland surveys, W. Abdalati for analysis of Greenland coastal meteorological data for temperature trends, and C. H. Davis and H. J. Zwally for providing their latest results from analysis of satellite radar-altimeter data. We wish to acknowledge the outstanding technical support of R. Mitchell, A. Waller, and J. Scott.

26 October 1998; accepted 2 January 1999

A Functional Model for O-O Bond Formation by the O₂-Evolving Complex in Photosystem II

Julian Limburg,¹ John S. Vrettos,¹ Louise M. Liable-Sands,² Arnold L. Rheingold,² Robert H. Crabtree,^{1*} Gary W. Brudvig^{1*}

The formation of molecular oxygen from water in photosynthesis is catalyzed by photosystem II at an active site containing four manganese ions that are arranged in di- μ -oxo dimanganese units (where μ is a bridging mode). The complex $[H_2O(terpy)Mn(O)_2Mn(terpy)OH_2](NO_3)_3$ (terpy is 2,2':6',2''-terpyridine), which was synthesized and structurally characterized, contains a di- μ -oxo manganese dimer and catalyzes the conversion of sodium hypochlorite to molecular oxygen. Oxygen-18 isotope labeling showed that water is the source of the oxygen atoms in the molecular oxygen evolved, and so this system is a functional model for photosynthetic water oxidation.

The O₂-evolving complex (OEC) in photosystem II (PSII) consists of a tetranuclear Mn cluster associated with Ca²⁺, Cl⁻, and a redox-active tyrosine that can effect the four-electron oxidation of water to dioxygen (1).

Extended x-ray absorption fine structure studies have shown that the Mn tetramer is made up of di- μ -oxo dimeric Mn units (μ is a bridging mode) (2). This assignment was made by a comparison with structural model

complexes, of which there are a large number (3). Although there are no di- μ -oxo Mn clusters that catalyze homogeneous O_2 evolution, there are two related systems that can effect homogeneous water oxidation (4, 5), and both are thought to proceed through a terminal oxo ligand of a high-valence metal ion $M=O$ (6). Correspondingly, a $Mn=O$ species has been proposed as an intermediate in photosynthetic water oxidation (7), where the terminal oxo ligand has been postulated to be formed by the abstraction of H atoms from a water molecule bound to Mn by the nearby tyrosyl radical (7, 8). Other mechanistic proposals for photosynthetic water oxidation have involved the reaction of bridging oxo units in a reaction that is analogous to that observed in a Cu dimer (1, 9). To test the former hypothesis, we designed a di- μ -oxo dimanganese complex with solvent coordination sites that provide a position for the formation of a $Mn=O$ intermediate. This strategy yielded a functional model of the OEC of PSII.

$Mn=O$, where the oxidation state of Mn is +4 or +5, has been identified as the reactive species in catalytic oxidations with Mn porphyrins (10) and has been proposed as the active species in catalysis with $Mn(salen)$ {where $salen$ is 1,3-bis[(2-hydroxybenzyl)imino]ethane} (11). There have also been three structurally characterized, albeit unreactive, $Mn(V)=O$ complexes (12). A water-oxidizing Ru dimer (13) operates through a reactive intermediate with a $Ru(V)=O$ group (14). There has been only one report of a Mn complex that can carry out homogeneous catalytic water oxidation—a face-to-face Mn diporphyrin, which has been proposed as forming a $Mn=O$ intermediate (5).

We had studied the reaction between potassium peroxomonosulfate (K oxone) and $Mn(II)$ and $Mn(III)$ complexes containing the planar tridentate ligands dipicolinate and terpyridine (15). Oxone was used because it had been successfully employed with Mn catalysts to oxidize organic compounds to give products that were consistent with $Mn=O$ intermediates (16). Our strategy was to study the reactivity of such intermediates in the absence of an organic substrate. We found that O_2 was produced catalytically and that the initial stage of the reaction involved the formation of di- μ -oxo dimanganese complexes, although we had been unable to isolate them. The catalyst was ultimately deactivated because the Mn was converted to

permanganate (17). Furthermore, no reactions were seen in controls using oxone with redox-inactive Lewis acids. Even with these controls, the use of oxone as an oxidant left a substantial amount of ambiguity in the mechanism because (although it has a predilection for O-atom transfer) it contains an O–O bond. Because of this, we proposed that the reaction involved a high-valence oxo intermediate but could not exclude the hydrolysis of a bound oxone. We found an analogous reaction between a structurally characterized Mn dimer and sodium hypochlorite (an O-atom transfer reagent that contains no O–O bond), and we also found the x-ray crystal structure of the catalyst precursor. To the best of our knowledge, this is the first clear example of an O–O bond-forming reaction involving a di- μ -oxo dimanganese complex that results in dioxygen evolution. Spectroscopic studies and ^{18}O isotope labeling are consistent with a mechanism involving a $Mn=O$ intermediate, and therefore, this system serves as a functional model for photosynthetic water oxidation.

Figure 1 shows an Oak Ridge thermal ellipsoid plot (ORTEP) of the $Mn(III)$ - $Mn(IV)$ complex $[OH_2(terpy)Mn(O)_2Mn(terpy)OH_2](NO_3)_3 \cdot 6H_2O$, referred to as **1** ($terpy$ is 2,2':6',2''-terpyridine) (18, 19). The unit cell contains two independent but chemically similar asymmetric units, and therefore, only one is shown here. Although the complex is a mixed-valence dimer, the two Mn units are crystallographically identical because the dimers are on inversion centers. The di- μ -oxo core has dimensions that are typical of such complexes

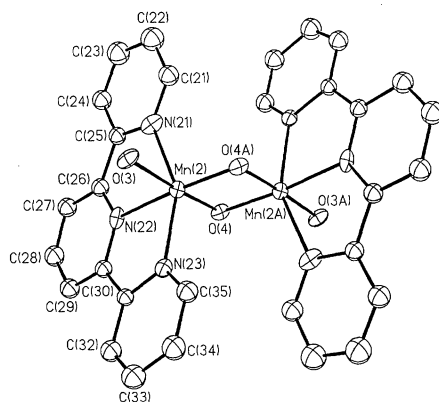


Fig. 1. An ORTEP diagram of **1**, showing ellipsoids of 30% probability. Hydrogen atoms, nitrate counterions, and waters of crystallization are omitted for clarity. Selected bond distances are as follows: $d(Mn2-Mn2A)$, 2.723(3) Å; $d(Mn2-O4)$, 1.812(6) Å; $d(Mn2A-O4)$, 1.811(7) Å; $d(Mn2-O4A)$, 1.811(7) Å; $d(Mn2-O3)$, 2.013(6) Å; $d(Mn2-N21)$, 2.100(8) Å; $d(Mn2-N22)$, 2.044(8) Å; and $d(Mn2-N23)$, 2.104(8) Å. Selected bond angles are as follows: $(O4A-Mn2-O4)$, 82.5(3) $^\circ$; $(Mn2-O4-Mn2A)$, 97.5(3) $^\circ$; $(O4-Mn2-O3)$, 176.5(3) $^\circ$; $(O4-Mn2-N22)$, 90.3(3) $^\circ$; $(O4A-Mn2-N22)$, 172.8(3) $^\circ$; $(O3-Mn2-N22)$, 93.1(3) $^\circ$; $(O4-Mn2-N21)$, 95.4(3) $^\circ$; and $(O4-Mn2-N23)$, 95.6(3) $^\circ$.

[for instance, the bond distance $d(Mn-Mn) \approx 2.7$ Å]. The most notable feature of the structure is the presence of an exchangeable aqua-coordination site on each of the Mn ions, which results from our use of the meridionally coordinating terpy ligand and which allows the complex to show the desired reactivity. The dimanganese complexes are wrapped in sheaths of H-bonding water molecules, which interlock the oxo bridges and coordinated water molecules. The two independent complexes show slightly different patterns of H bonding.

When the mixed-valence dimer **1** (12.5 μ M in water) was added to a solution of 0.07 M NaClO (pH = 8.60), O_2 evolved with an initial rate of 12 ± 2 mol hour $^{-1}$ per mol of **1** and four catalytic turnovers in total (Fig. 2) (20). We have followed the O_2 evolution in a He atmosphere using ^{18}O labeling with an analysis of the products by mass spectrometry (21). Because CO_2 (present as an adventitious background gas) rapidly exchanges with $H_2^{18}O$, the ^{18}O content of the CO_2 was a good measure of the isotopic content of the water. The ratio $^{48}CO_2:^{46}CO_2$ was found to be the same as the ratio $^{36}O_2:^{34}O_2$ (1.49 ± 0.05 versus 1.48 ± 0.03 , which is the average of two independent measurements), demonstrating quantitative incorporation of solvent-derived O atoms into O_2 . The measured ratios of the bis- ^{18}O and $^{18}O^{16}O$ compounds correspond to an ^{18}O content of the water of 75%; this agrees with the calculated content after dilution (21). A control experiment in the absence of catalyst showed that the intrinsic exchange rate of hypochlorite with water is slow under the reaction conditions (21).

Oxygen-18 exchange has been proposed as evidence for the participation of $Mn(V)=O$ species in oxidation chemistry involving water-soluble Mn porphyrin complexes with exchangeable coordination sites (10, 22). Exchange with a $Mn(V)=O$ intermediate by the mechanism proposed by Bernadou and Meunier (22) was expected to be relatively rapid in our system, as there would be a water or hydroxide ligand coordinated to the terminal oxo-containing complex. This mechanism can account for the observed isotopic distribution of the O_2 that was formed from catal-

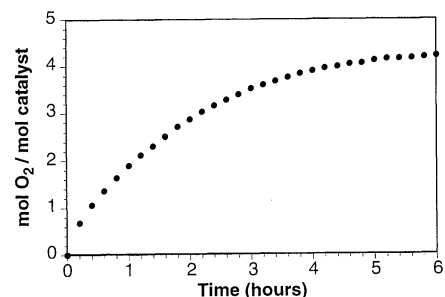


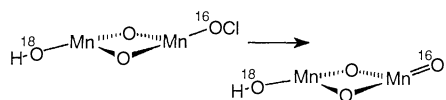
Fig. 2. O_2 evolution versus time for a solution containing 0.05 μ mol of **1** in 4 ml of 0.07 M NaClO at pH = 8.6 ($[1] = 12.5$ μ M).

¹Department of Chemistry, Yale University, Post Office Box 208107, New Haven, CT 06520-8107, USA.

²Crystallography Laboratory, Department of Chemistry, University of Delaware, Newark, DE 19716, USA.

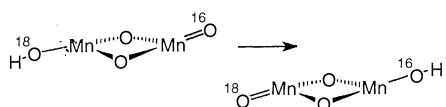
*To whom correspondence should be addressed. E-mail: robert.crabtree@yale.edu; gary.brudvig@yale.edu

ysis in our system. We envisage the first step as being the formation of a Mn=O, where the O atom originates from $^{16}\text{OCl}^-$ (Scheme 1a).



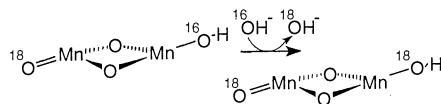
Scheme 1a.

The terminal oxo ligand can then rapidly exchange with a ^{18}O -labeled hydroxide or aqua ligand on the other Mn ion of the dimer (Scheme 1b). Finally, the ^{16}O -hydroxide/



Scheme 1b.

aqua ligand that subsequently forms can then rapidly exchange with the solvent to produce a complex where both Mn sites are ^{18}O labeled (Scheme 1c), a requirement for quanti-



Scheme 1c.

tative label incorporation from water into O_2 .

The Mn=O can be thought of as either an electrophile (7) (and therefore open to attack by a OH^- that may be either free or ligated to a second Mn dimer) or as a radical species (7) that could react with a water molecule from outside the complex. Either of these pathways would result in O_2 whose isotopic composition would match that of the solvent. Another possibility is the exchange of ^{18}O into and out of the bridging oxo units.

The catalytic reactions end with the complete conversion of the Mn to permanganate after ~ 6 hours. The formation of permanganate can be followed by ultraviolet-visible (UV-vis) spectroscopy (Fig. 3) (23). Isosbestic points at 497 and 583 nm, which show

direct conversion of the major species in solution to permanganate, appear when the reaction has reached steady state (time $t > 1$ min). Permanganate presumably forms through a disproportionation of the reactive species, and this step would require the oxidation of 1 above the IV/IV state to be coupled to O-atom transfer.

For over 1 hour, we followed the total number of oxidizing equivalents in a solution containing 0.07 M NaClO and 75 μM 1. About 10 times more hypochlorite was consumed than could be accounted for by O_2 evolution, suggesting that a substantial amount of ligand oxidation had occurred. The data were obtained by taking 20- μl aliquots of the reactive solution, quenching them in 20 ml of 0.1 M KI, and then using the visible absorbance at 360 nm to quantify the amount of I_3^- that was formed (24). Permanganate formation requires that the free ligand be released into solution, and so, oxidation of this ligand (either hypochlorite or Mn based)

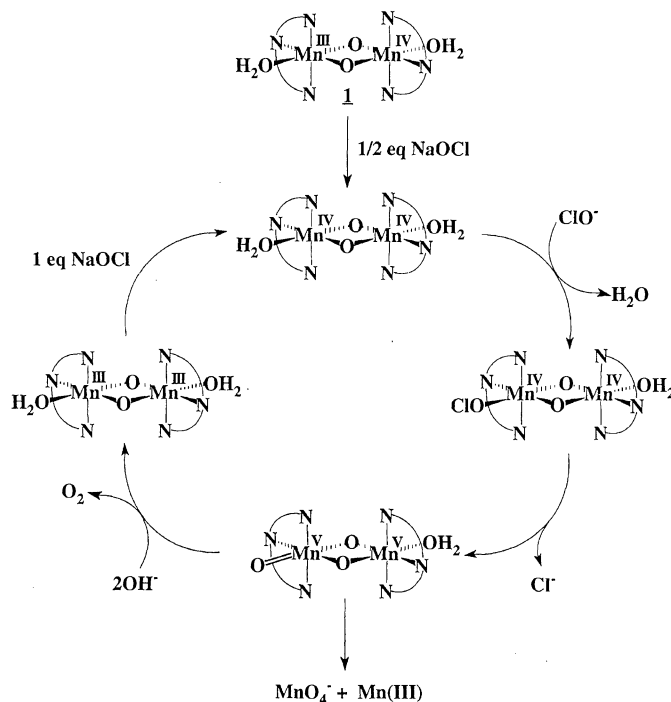
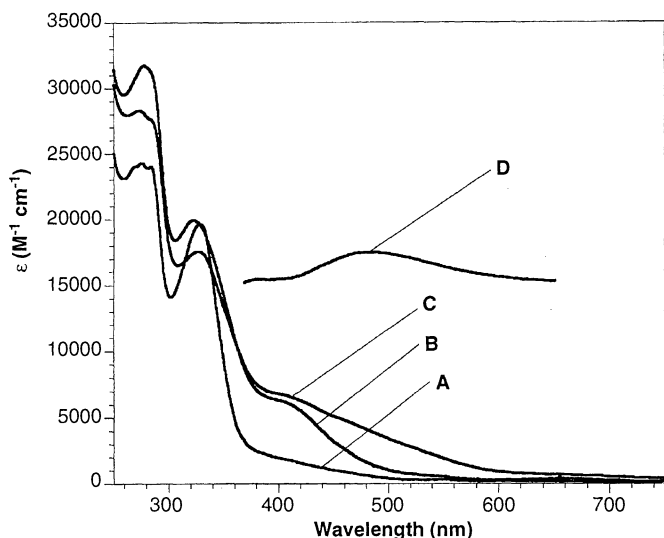
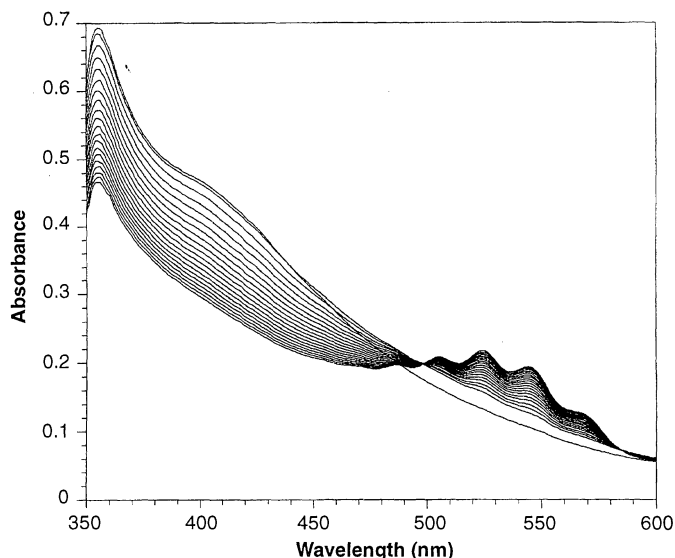


Fig. 3 (top left). Time course of UV-vis absorbance changes during the reaction between 100 μM 1 and 0.25 M NaClO (pH = 8.6), from $t = 0$ to 17 min. Spectra are shown with $\Delta t = 1$ min, and there are isosbestic points at 497 and 583 nm that appear after the first minute. Fig. 4 (bottom left). Comparison of the UV-vis spectra. (A) 50 μM 1 in water, (B) 50 μM IV/IV dimer in water [see (25)], (C) 50 μM 1 in 0.07 M NaOCl (pH = 8.6), and (D) the difference spectrum between (C) and (B) showing the visible absorbance of C at 480 nm. Fig. 5 (above). A simplified proposal for the reaction mechanism of the formation of O_2 from the reaction of 1 with NaClO. A Mn(V)=O dimer is produced by the oxidation of the IV/IV dimer, and then, the O-O bond-forming step could involve a nucleophilic attack of OH^- on the oxo group. Permanganate would form by the disproportionation of the V/V dimer.

may be partially responsible for the loss of oxidizing equivalents.

Figure 4 shows a comparison of the UV-vis spectra of **1**, the IV/IV dimer (**25**), and the catalytic solution at $t = 0$. These spectra indicate that the catalytic solution contains a small amount of IV/IV dimer (**26**), but the solution also contains another species that has a relatively strong absorbance in the visible region at ~ 480 nm. The visible absorbance band associated with this species probably arises from a ligand-to-metal charge-transfer transition (**26**). There are various possible sources for this band, such as a Mn=O-containing complex.

Electron paramagnetic resonance (EPR) spectra of frozen aliquots of a 50 μ M solution of **1** in hypochlorite over the first hour of the reaction show no signals (the samples were frozen at 5-min intervals), indicating that the major species is either diamagnetic or has integer spin (**27**). An EPR spectrum of complex **1**, which has a 16-line spectrum that is characteristic of mixed-valence dimers (**28**), is readily obtainable under comparable conditions. This result provides support for the major species in solution as being a IV/IV or a V/V dimer, as these would be expected to show no signals from EPR.

Figure 5 shows a simplified mechanism for O₂ formation from the reaction of **1** with sodium hypochlorite. The EPR and optical studies indicate that **1** initially reacts rapidly to form the IV/IV dimer with no EPR signals and that this is the major species involved in catalysis. The IV/IV dimer can then react with sodium hypochlorite to form a Mn(V)=O intermediate, and this is the species that is featured in the O–O bond-forming step. The proposed mechanism for O–O bond formation involves an attack of OH[–] on the Mn=O to form a peroxy intermediate that then rapidly reacts with two further oxidizing equivalents and releases O₂. Permanganate would form in a competing reaction by disproportionation of the Mn(V/V) intermediate to give Mn(VII) and Mn(III).

References and Notes

1. V. K. Yachandra, K. Sauer, M. P. Klein, *Chem. Rev.* **96**, 2927 (1996); R. J. Debus, *Biochim. Biophys. Acta* **1102**, 269 (1992); B. A. Diner and G. T. Babcock, in *Oxygenic Photosynthesis: The Light Reactions* vol. 4 of *Advances in Photosynthesis*, D. R. Ort and C. F. Yocum, Eds. (Kluwer Academic, Dordrecht, Netherlands, 1996), pp. 214–240; R. D. Britt, *ibid.*, pp. 137–159.
2. V. K. Yachandra *et al.*, *Science* **260**, 675 (1993).
3. R. Manchanda, G. W. Brudvig, R. H. Crabtree, *Coord. Chem. Rev.* **144**, 1 (1995); K. Wieghardt, *Angew. Chem. Int. Ed. Engl.* **33**, 725 (1994).
4. D. Geselowitz and T. J. Meyer, *Inorg. Chem.* **29**, 3894 (1990).
5. Y. Naruta, M. Sasyama, T. Sasaki, *Angew. Chem. Int. Ed. Engl.* **33**, 1839 (1994).
6. W. Rüttinger and G. C. Dismukes, *Chem. Rev.* **97**, 1 (1997); J. Limburg, G. W. Brudvig, R. H. Crabtree, in *Biomimetic Oxidations Catalyzed by Transition Metals*, B. Meunier, Ed. (World Scientific, Singapore, in press).
7. C. Tommos *et al.*, *Curr. Opin. Chem. Biol.* **2**, 244 (1998); C. W. Hoganson and G. T. Babcock, *Science*

- 277**, 1953 (1997); D. W. Randall *et al.*, *J. Am. Chem. Soc.* **117**, 11780 (1995); J. Messinger, M. Badger, T. Wydrzynski, *Proc. Natl. Acad. Sci. U.S.A.* **92**, 3209 (1995); P. E. M. Siegbahn and R. H. Crabtree, *J. Am. Chem. Soc.* **121**, 117 (1999); J. Limburg, V. A. Szalai, G. W. Brudvig, *J. Chem. Soc. Dalton Trans.*, in press; V. L. Pecoraro, M. J. Baldwin, M. T. Caudle, W. Hsieh, N. A. Law, *Pure Appl. Chem.* **70**, 925 (1998); M. L. Gilchrist, J. A. Ball, D. W. Randall, R. D. Britt, *Proc. Natl. Acad. Sci. U.S.A.* **92**, 9545 (1995).
8. M. J. Baldwin and V. L. Pecoraro, *J. Am. Chem. Soc.* **118**, 11325 (1996); M. R. A. Blomberg *et al.*, *ibid.* **119**, 8285 (1997).
9. J. A. Halfen *et al.*, *Science* **271**, 1397 (1996); V. L. Pecoraro, M. J. Baldwin, A. Gelasco, *Chem. Rev.* **94**, 807 (1994).
10. J. T. Groves and M. K. Stern, *J. Am. Chem. Soc.* **110**, 8628 (1988); J. T. Groves, J. Lee, S. S. Marla, *ibid.* **119**, 6269 (1997).
11. S. F. Finney *et al.*, *Angew. Chem. Int. Ed. Engl.* **36**, 1720 (1997).
12. T. J. Collins and S. W. Gordon-Wylie, *J. Am. Chem. Soc.* **111**, 4511 (1989); T. J. Collins, R. D. Powell, C. Slobodnick, E. S. Uffelman, *ibid.* **112**, 899 (1990); F. M. MacDonnell, N. L. P. Fackler, C. Stern, T. V. O'Halloran, *ibid.* **116**, 7431 (1994).
13. S. W. Gersten, G. J. Samuels, T. J. Meyer, *ibid.* **104**, 4029 (1982).
14. J. K. Hurst, J. Zhou, Y. Lei, *Inorg. Chem.* **31**, 1010 (1992).
15. J. Limburg, G. W. Brudvig, R. H. Crabtree, *J. Am. Chem. Soc.* **119**, 2761 (1997).
16. J. Bernadou, A.-S. Fabiano, A. Robert, B. Meunier, *ibid.* **116**, 9375 (1994); J. Wessel and R. H. Crabtree, *J. Mol. Catal.* **133A**, 13 (1996).
17. In (**15**), we stated that when terpy was used, permanganate was not formed. However, we later found that permanganate was being produced in substoichiometric amounts.
18. All chemicals were purchased from Aldrich and were used without further purification. Synthesis of **1** was as follows. Mn(II)(OAc)₂ (1.060 g and 4.29 mmol) (OAc, acetate) and terpy (1.000g, 4.29 mmol) were dissolved in 15 ml of water (pH = 7), and K oxone (standardized as 0.289 mmol per 100 mg, 1.110 g, and 3.21 mmol) in 15 ml of water was added dropwise with stirring, causing the yellow solution to turn dark green. After stirring at room temperature for 10 min, the solution was cooled to 0°C, 20 ml of a saturated KNO₃ solution were added, and a green solid precipitated out, which was collected by filtration and washed three times with 5 ml of iced water and then washed three times with 5 ml of ether. After drying in a vacuum, the yield was 1.361 g (76% on the basis of ligand). Spectroscopy data are as follows: Infrared (cm^{–1}) (KBr): 3070 (m, br), 1599 (s), 1477 (s), 1383 (vs), 1287 (m), 1017 (m), 779 (m), and 703 (m); absorptions are indicated as m, medium; br, broad; s, strong; and vs, very strong. The calculated elemental analysis for 1·3H₂O was C, 40.63%; H, 3.83%; and N, 14.22%. We found the elemental analysis to be C, 40.76%; H, 3.70%; and N, 14.03%. Crystals suitable for x-ray analysis were obtained by evaporation of 1 ml of a filtered 20 mM solution of **1** placed in a 15-ml round-bottomed flask. A black blade-like crystal with dimensions of 0.50 mm by 0.20 mm by 0.02 mm was mounted and analyzed with a Bruker system. Crystal data are as follows for 1·6H₂O: C₃₀H₄₀Mn₂N₉O₁₉; molecular weight $M_w = 940.59$; triclinic crystal system; space group $P\bar{1}$; unit cell edges $a = 7.6196(2)$ Å, $b = 13.7393(4)$ Å, and $c = 19.4569(6)$ Å; interaxial angles $\alpha = 74.2995(12)^\circ$, $\beta = 87.3068(12)^\circ$, $\gamma = 79.9959(12)^\circ$; cell volume $V = 1931.08(14)$ Å³; formula units per cell $Z = 2$; temperature $T = 173(2)$ K; calculated density $D_{\text{calc}} = 1.614$ g cm^{–3}; absorption coefficient $\mu(\text{Mo K}\alpha) = 0.71073$ Å^{–1} = 7.46 cm^{–1}; and residuals $R(F) = 9.71\%$ for 2501 independent reflections ($4^\circ \leq 2\theta \leq 46^\circ$); standard errors in the last decimal place are given in parentheses. In the asymmetric unit, there are two half dimers (each on an inversion center), three nitrate ions, and six water molecules. Despite several at-

tempts at recrystallization, the best crystals that could be obtained were very weak x-ray scatterers (intensity-to-background ratio $I/\sigma = 2.20$). All C atoms were refined isotropically to maintain a reasonable data-to-parameter ratio. The H atoms on the aqua ligands and lattice water molecules could not be located from the difference map and were ignored. All other H atoms were treated as idealized contributions. All software sources of the scattering factors are contained in the SHELXTL 5.1 library (Siemens X-ray Diffraction, Madison, WI). The crystal structure data has been deposited at the Cambridge Crystallographic Data Centre (CCDC 113788).

19. This complex has been independently synthesized (M.-N. Collomb, A. Deronzier, A. Richardot, J. Pecaut, *New J. Chem.*, in press).
20. Sodium hypochlorite (5% and 10 to 13%) was purchased from Aldrich and standardized by iodometric titration. Measurements of O₂-evolution were made with a YSI standard oxygen probe attached to a strip-chart recorder. In a catalytic run, 4 ml of 0.07 M NaClO (pH = 8.6) solution were stirred under the electrode in an airtight system, and an appropriate volume of **1** (1 mM in water at pH = 7) was added from a gastight syringe by means of a small channel along the side of the Teflon-coated holder. Initial rates were calculated for $t = 0$ to 2 min.
21. In a typical experiment, 25 μ l of a 10 mM solution of **1** and 25 μ l of a 1 M solution of NaClO (pH adjusted to 8.6 with HNO₃) were placed in separate sides of a two-bulb flask (each bulb had a volume of ~ 15 ml). Ninety-five percent H₂¹⁸O (250 μ l) was then added to the solution of **1**, and then, both solutions were thoroughly degassed by three freeze-pump-thaw cycles. The two solutions were then mixed in a vacuum, and O₂ evolution was allowed to occur for 1 hour, at which time the solution was frozen and the head-space gas was drawn into an evacuated 150-ml metal cylinder. The gas was then analyzed with a HP 5989A mass spectrometer. To test the intrinsic exchange rate of NaOCl, we diluted 25 μ l of 1 M NaOCl to 275 μ l with 95% H₂¹⁸O. One hour after mixing, the OCl[–] was extracted into 1 ml of CH₂Cl₂, containing 0.025 M tetra-*n*-butylammonium hydrogen sulfate, and dried with magnesium sulfate. The (*n*-Bu)₄N⁺OCl[–] was then quenched with two equivalents of thioanisole, and the resulting solution was characterized by mass spectrometry. The ¹⁸O content of the methylphenylsulfonoxide was ascertained with the ratio of the fragments at the mass/charge ratios 125 and 127, owing to an interfering mass at 142 from the (*n*-Bu)₄N⁺ ion, and was equivalent to 40% incorporation into NaOCl.
22. J. Bernadou and B. Meunier, *J. Chem. Soc. Chem. Commun.* **1998**, 2167 (1998).
23. UV-vis spectra were taken with an HP 8453 diode array spectrophotometer. For the time-course experiment, 2.5 ml of 200 μ M **1** was added to 2.5 ml of 0.5 M NaClO (pH = 8.6); the solution was then mixed and rapidly transferred to a cuvette. For the scans to 280 nm, a 1-mm-pathlength cuvette was used; as with longer pathlengths, the hypochlorite absorbance below 350 nm interfered with the absorbance from the Mn complex.
24. T. C. Bruce, J. B. Noar, S. S. Ball, U. V. Venkataram, *J. Am. Chem. Soc.* **105**, 2452 (1983).
25. The IV/IV dimer [(SO₄)₂(terpy)Mn(O)₂Mn(terpy)(SO₄)₂·3H₂O] was isolated and crystallographically characterized (J. Limburg *et al.*, unpublished results), but because **1** is much more soluble, it is more convenient to use for the reactivity studies.
26. D. R. Gamelin *et al.*, *J. Am. Chem. Soc.* **116**, 2392 (1994).
27. EPR spectra were recorded on frozen solutions at 10 K with a Varian E-9 X-band spectrometer with a He cryostat at an applied microwave power of 5 mW.
28. H. H. Thorp and G. W. Brudvig, *New J. Chem.* **15**, 479 (1991).
29. This work was funded by NIH grant GM32715. The authors thank M.-N. Collomb for communicating experimental data before publication.

13 November 1998; accepted 3 February 1999